

Rhythms of the collective brain: Metastable synchronization and cross-scale interactions in connected multitudes

Miguel Aguilera^{1,2,*}

¹Department of Computer Science and Systems Engineering, University of Zaragoza, Zaragoza, 50018, Spain

²Department of Psychology, University of the Balearic Islands, Palma de Mallorca, 07122, Spain

*sci@maguilera.net

ABSTRACT

Collective social events operate at many levels of organization – from individuals to crowds – presenting a variety of temporal and spatial scales of activity, whose causal interactions challenge our understanding of social systems. Large data sets of social media activity provide an unprecedented opportunity to investigate the processes that govern the coordination within and between those scales. Using as a case study a data set comprising 1.5 million Twitter messages of the activity around the 15M movement in Spain as an example of multitudinous self-organization, we propose a generic description of the coordination dynamics of the system based on phase-locking statistics at different frequencies using wavelet functions, identifying 8 frequency bands of entrained oscillations between 15 geographical urban nodes. We apply maximum entropy inference methods to extract Ising models capturing phase-locking activity between geographical nodes in our data at each frequency band. Inspecting the properties of the resulting models for each frequency we show that 1) all frequency bands of the system are operating in a regime of criticality and 2) while fast frequencies present only a few metastable states displaying all-or-none synchronization, slow frequencies present a variety of metastable states displaying distinct modes of partial synchronization. Furthermore, describing states of coordination at each frequency using the energy function inferred for each Ising model, we use symbolic transfer entropy to characterize cross-scale interactions between frequency bands, showing 1) a cascade of upward information flows in which each frequency band influences its contiguous slower frequency bands and 2) downward information flows where slow frequencies modulate distant fast frequencies.

Introduction

Coordinated activity is a powerful force in creating and sustaining human communities together [1]. From communal dances in ancient human groups to civic festivals in the French Revolution or muscular manifestations in Nazi marches and rallies [1, p.136, p.148-149], visceral and emotional sensations of shared movement have historically been used to create a sense of community and to shape the public expression to communal or political shared principles. With the development of communication technologies, new forms of coordination for large and scattered communities have become available. Interestingly, forms of distributed communication and coordination have often come together with episodes of large-scale mobilization and social change, as the widespread print-shop networks of radical reforming movements with the generalization of the printing press during the 16th century German Reformation [2] or postal networks during the Republic of Letters in the 17th and 18th centuries [3].

Today, the rise of new digital communication tools and network technologies is pushing forward fast bidirectional communication, generating new forms of collective communication and action. Digital communications increase the autonomy and influence of the social groups using them facilitating forms of mass self-communication [4], collective intelligence using pools of social knowledge [5] or *smart mobs* taking advantage of the communication and computing capabilities of widespread technological devices [6]. From protest movements like the Arab Spring or the Occupy movements to autonomous responses to natural disasters like Hurricane Sandy or the Tōhoku earthquake, several examples highlight the increasing capacity of social and political grassroots organizing displayed by multitudes connected through digital medial. With the popularity of social media, a trendy topic of discussion focuses on the large-scale coordination self-organized of connected multitudes: how they arise and ensemble, what mechanisms lie underneath their organization and how are they able to constitute autonomous social and political subjects [7]. In this debate, some positions argue that digital communication tools promote a individualistic logic based on sharing personalized content through social media which is distinct to earlier forms of collective actions linked to more rigid organizational structures and collective identities [8]. In contrast, other views argue that digital communication brings about the primacy of processes of aggregation as a *reductio ad unum* of the complexity of the social [9, 10]. Alternatively,

asides from individualized action or global aggregation, one could consider that similarly to biological brains, what constitutes social collective ‘brains’ as complex entities is their capacity to display coordination at multiple scales, perhaps in a manner that is not so different from neural large-scale synchronization over multiple frequency bands [11, 12]. Along similar lines, recent work about collective identities in connected multitudes emphasizes the interaction between levels and the role of mesoscale levels of activity in order to capture the multiplicity, changing nature and diversity of the interactions between singular actors, groups and collective initiatives [13]. In any case, the principles operating behind networks of connected multitudes require further conceptual and experimental contributions in order to address these and other theoretical questions.

Luckily, the rise of social media and digital data-mining brings as well the opportunity for a genuine analysis and synthesis of human social life [14] explaining the behaviour of social systems at distinct levels of description and unveiling the interactions between these different scales. This provides the opportunity to shed light on theoretical debates providing hypothesis based on inference from real data. Nonetheless, this endeavour is not extent of difficulties. A particularly difficult task is conceiving and describing the exchanges between different levels of description of social systems. From individual to group behaviour, social systems operate on many levels of organization, being their temporal and spatial scales interwoven together in a complex network of interactions, where causal relations between levels are often difficult to capture.

Here, we use Twitter data to analyse and model phase-locking dynamics between geographically distant urban regions at different frequency bands, with the objective of inferring theoretical models explaining interactions within and between temporal scales. In particular, we use a well known social event of large-scale social and political self-organization: the massive political protest of the 15M movement in Spain, emerging in the aftermath of the Arab Spring of 2011. The case of the 15M movement is interesting for a number of reasons. First, it consists in a self-organized social movement arising from online communication in a decentralized network of citizens and civil associations (without any coverage of mainstream media until time after the protests took the streets). Second, the movement led to massive demonstrations and camps throughout all the country, creating a collective agency which has had a profound impact in Spanish politics in the subsequent years [15–17]. Finally, a series of studies have characterized some of the emerging properties of the 15M and how it exhibits features typical of critical systems and others suggesting distributed self-organization [18–20].

Using a data set of 1.5 million messages, we analyse the interactions between geographical urban nodes within and between temporal scales. First, we use phase-locking statistics at different frequencies using wavelet functions, identifying 8 frequency bands showing salient synchronization levels. For each frequency band, we extract an Ising model as the least structured, or maximum-entropy, probability distribution reproducing pairwise correlations found in phase-locking dynamics of the data at the correspondent synchronization frequency. Inspecting the properties of the resulting models at each frequency band we show that 1) all frequency bands of the system are operating at a regime of criticality and 2) while fast frequencies present only a few metastable states of all-or-none synchronization, slow frequencies present a variety of modes of partial synchronization as metastable states. Furthermore, using the Ising models to represent the energy of the configurations found in the data, we characterize cross-scale interactions measuring symbolic transfer entropy between frequency bands. We describe the relation between the energy configuration at different frequency bands showing 1) a cascade upward information flows in which each frequency band only influences its contiguous slower band and 2) and long-range downward information flow where slow frequency bands directly modulate distant faster bands.

Results

We use a data set of 1,444,051 time-stamped tweets from 181,146 users, collected through the Twitter streaming API between 13 May 2011 and 31 May 2011 [16]. Messages were captured during 17 days during the Spanish 15M social unrest events in 2011, capturing messages containing at least one of a set of 12 keywords or hashtags related to the protest (see reference 16 for a detailed description). We extracted geographical information from the location information of users (see Methods), selecting the 15 urban areas with largest number of messages. Using this information, we generated time-stamped series reflecting the number of tweets emitted from each city for intervals of 60 seconds.

Synchronization at multiple frequencies

One of the most prominent features of the 15M movement was its fast territorial development. Without any coordination centre or any formal organization, the movement was able to reproduce a network of camps across Spanish cities in a period of a few days. In order to analyse the coordination between populations at main Spanish cities we use Morlet wavelet filtering to extract the phase content $\theta_i(f, t)$ of the activity time series at city i at time t and frequency f , using a span of frequencies in the range $[1.67 \cdot 10^{-3} \text{Hz}, 9.26 \cdot 10^{-5} \text{Hz}]$ (from 10 minutes to 3 hours) logarithmically distributed with intervals of $10^{0.01}$. We use phase

locking statistics [21] to define phase locking values between two cities i and j as:

$$\phi_{ij}(f, t) = \left| \frac{1}{\delta} \sum_{\tau=-\delta/2}^{\delta/2} e^{i(\theta_y(f, t+\tau) - \theta_x(f, t+\tau))} \right| \cdot A_{ij}(t) \quad (1)$$

where δ is the size of the window of temporal integration: $\delta = \frac{n_c}{f}$, being n_c the number of cycles in which we analyse phase-locking. We use a value of $n_c = 8$ cycles, similar to the values typically used in neuroscience, ensuring that we are detecting sustained synchronization. $A_{ij}(t)$ is a corrector factor which removes spurious synchronization when the network is inactive (e.g. during nighttime, see Methods).

Statistical significance of phase locking values is determined by comparing it to phase locking values of surrogate time series obtained using the amplitude adjusted Fourier transform [22]. We use 200 surrogate time series to estimate a significance threshold for the values of $\phi_{ij}(f, t)$ for all values of f . The average phase locking values of surrogate time series were used to compute a threshold $\phi_{th}(f)$, indicating a value higher than 99% of surrogate data. Using this threshold, we define phase locking links between two cities i and j as statistically salient values of $\phi_{ij}(f, t)$:

$$\Phi_{ij}(f, t) = \begin{cases} 1, & \text{if } \phi_{ij}(f, t) \geq \phi_{th}(f) \\ 0, & \text{otherwise} \end{cases} \quad (2)$$

Using this technique we find widespread moments of statistically significant synchrony at different frequencies and temporal moments. In reference 23 we have documented how instants of synchrony correspond to significant moments of the 15M protests. For illustrative purposes, in Figure 1 we show the total number of phase locking links $S(f, t) = \sum_{i,j} \Phi_{ij}(f, t)$ for a specific day of the protests: May 27th. We observe how clusters of synchronized cities arise at different frequencies and moments of time. At faster frequencies (lower period) we observe short and less intense instants of synchrony, while at slower frequencies synchrony last for longer periods of time. Figure 1 corresponds to one of the days with most intense protest activity, in which the police violently evicted a demonstrators' encampment at Barcelona, which was subsequently recovered by a multitude of peaceful protesters. Elsewhere [23], we have shown how the interaction between the two lower frequencies bands of synchronization allows the network to engage in two complementary modes of activity. The first mode corresponds to the network of cities focused in the events happening in Barcelona and the second one reflects a nationwide protest in solidarity with Barcelona organized from other cities. An analysis of transfer entropies between the phases of the activity at each city for the frequencies of both synchronized coalitions shows how the system is operating quite differently for each one (Figure 2). While one coalition is led by the node of Barcelona, with information flowing from this node to others, the second coalition presents a more distributed flow of information (for a detailed description of the analysis see reference 23).

Pairwise maximum entropy modelling of phase-locking statistics

In order to inspect how these phase-locked coalitions are operating at each frequency band, we derive from our data a statistical model of the system. Using maximum entropy models we infer the probability distribution of possible states of the network, corresponding to all the combinations of binary possibilities of each node being or not phase-locked to other nodes of the network at a particular frequency of synchronization. For simplicity, we consider the state of a node i being phase-locked to a synchronized cluster, that is $s_i = 1$, when it has at least one synchronization link and (i.e. $\Phi_{ij} = 1$ for at least one value of j), and otherwise the state of the node is set to $s_i = -1$. We extract a pairwise maximum entropy model described by the Boltzmann distribution of an Ising model. This is the least-structured model that is consistent with the mean activation rate and correlations of the nodes of the network. Pairwise correlation maximum entropy models have been successfully used to map the activity of networks of neurons [24], antibody sequences [25] or flocks of birds [26]. These models, instead of being postulated as approximations of real phenomena, can infer exact mappings capturing measured properties of a system reflected in the applied constraints (means and correlations in our case). This makes them good candidates to capture the structures underlying social coordination.

The maximum entropy distribution consistent with a known average energy is the Boltzmann distribution $P(s) = Z^{-1} e^{-\beta E(s)}$, where s is a state of the network, Z is the partition function and $\beta = \frac{1}{T k_B}$, being k_B Boltzmann's constant and T the temperature. The energy of the model with pairwise interactions is defined as $E(s) = -\sum_i h_i s_i - \frac{1}{2} \sum_{i < j} J_{ij} s_i s_j$, where 'magnetic fields' h_i represent influences in the activation of individual nodes and 'exchange couplings' J_{ij} stand for the tendencies to correlated activity between nodes. Without loss of generality we can set the temperature $T = 1$. Considering a pairwise model, the resulting distribution of the maximum entropy model is:

$$P(s) = \frac{1}{Z} \exp \left[\beta \sum_i h_i s_i + \frac{1}{2} \sum_{i < j} J_{ij} s_i s_j \right] \quad (3)$$

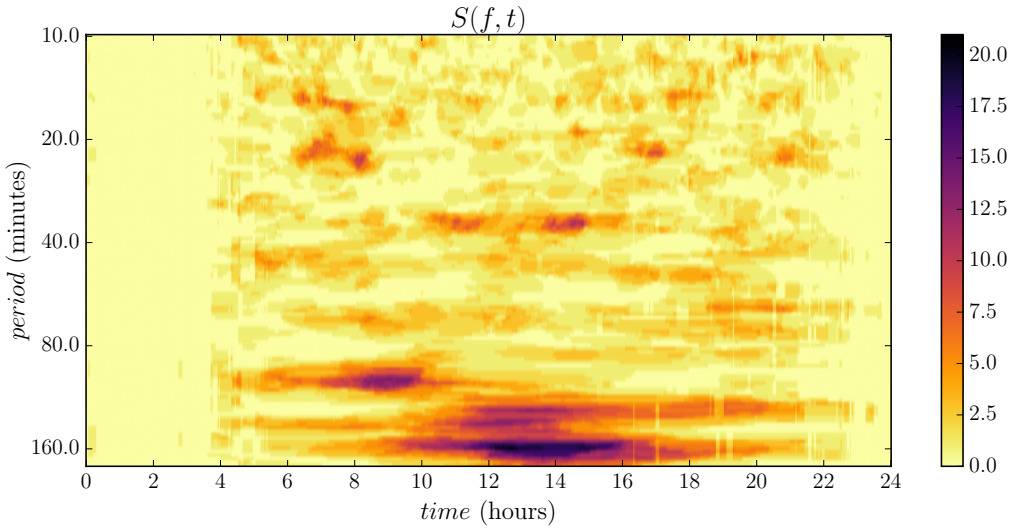


Figure 1. Phase locking statistics. Sum of the number of phase locking links between all cities $S(f, t)$ for day May 27. The horizontal axis represents a temporal span of instants t during the day, and the vertical axis represents the period corresponding to the frequency f of the wavelets used for extracting phase contents of the signals. The colour represents the sum of phase locking links for f and t .

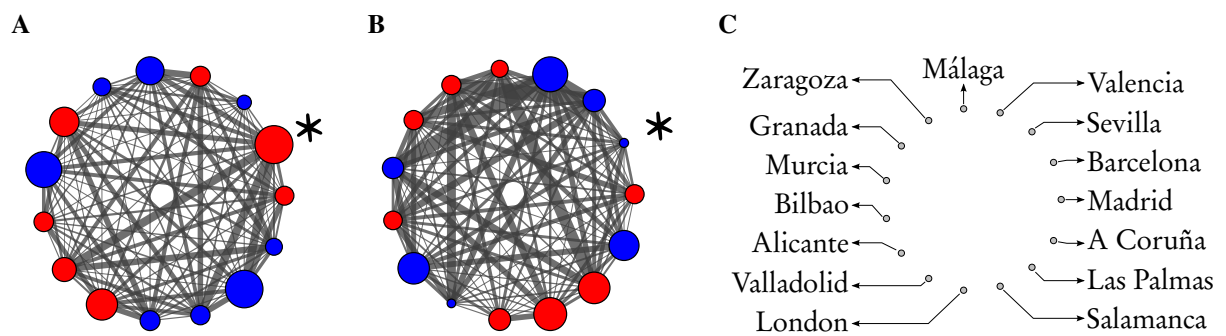


Figure 2. Integration flows in phase-locked coalitions for day May 27. Networks (A) and (B) represent symbolic transfer entropy between the phase relations of the nodes at the two slower synchronization frequencies found in Figure 1. (C) displays the positions of the analysed cities in the network. The width of the edges represent the relative transfer entropy between pairs of nodes. The size of the node represents the absolute mean relative transfer entropy between one node and the others, and the colour represents the sign of the mean relative transfer entropy. Red nodes characterize information sources, and blue nodes represent information sinks. While for the frequency represented in network A distributes information preferentially from Barcelona (marked with an asterisk) to other nodes, information flows in network B are distributed more homogeneously. A detailed description of this figure can be found in reference 23.

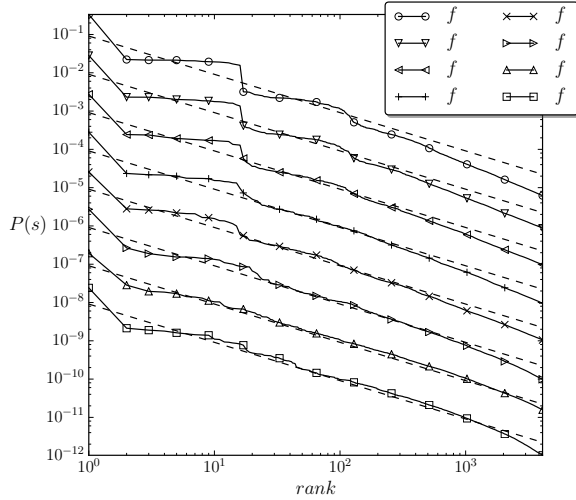
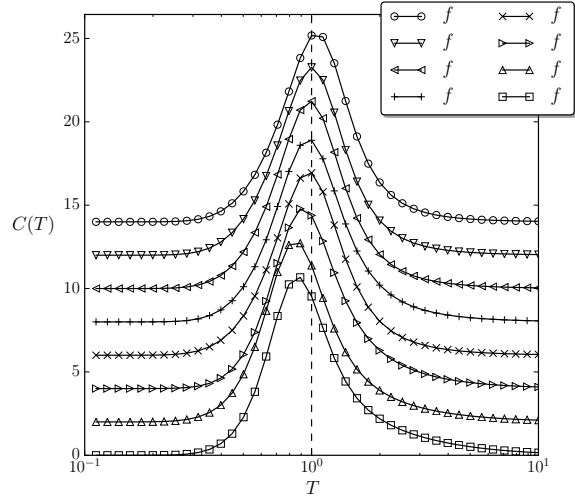
A**B**

Figure 3. Signatures of criticality. (A) Ranked probability distribution function of the inferred Ising models for the different frequency bands (solid line) versus a distribution following Zipf's law, (i.e. $P(s) = 1/rank$, dashed lines). We observe a good agreement between the model and Zipf law, suggesting critical scaling. (B) Heat capacity versus temperature for the inferred Ising models for different frequency bands. Temperature $T = 1$ is the point where our models are poised, coinciding with a divergence of the heat capacity, which is a classical signature of criticality. In both graphs lines are added an offset value in order to facilitate visualization of the distinct frequencies.

where the h_i and J_{ij} are adjusted to reproduce the measured mean and correlation values between nodes of the network (see Methods).

Using wavelet pattern matching [27] for detecting peaks of synchronization links (see Methods and Supplementary Information), we select eight representative frequency bands f_k , $k = 1, \dots, 8$, where larger k corresponds to larger timescales (i.e. slower frequencies). From these frequency bands we extract models of pairwise correlations at the corresponding frequencies. For each frequency band, we infer an Ising model $P_{f_k}(s)$, using a coordinate descent algorithm (see Methods) for fitting the parameters h_i and J_{ij} that reproduce the means and correlations found in the series of states s for the description of phase-locking relations at each frequency.

The accuracy of the inferred models can be evaluated by asking how much of the correlation structure is captured. One measure to evaluate this is the ratio of multi-information between the model and real data [28]. In our case, our data limits ourselves to compute the entropy of small sets of nodes (between 5 and 7, see Supplementary Information). Limiting our entropy calculations to random sets of five to seven nodes, we can see in Figure S2 and Table S3 that our models are able to capture around 70% of the correlations in the data, indicating a good performance of the model for the correlations of subsets of the indicated sizes. A more detailed description of multi-information analysis for characterizing the accuracy of the model can be found in the Supplementary Information.

Once we have extracted a battery of models $P_{f_k}(s)$, indicating the probability distributions of phase-locking configurations at different frequency bands, we explore the thermodynamics associated to them. First, we observe how all the models are poised at critical points. One signature of criticality we find is that the probability distribution of $P_{f_k}(s)$ follows a Zipf's law (Figure 3.A), specially for slower values of f_k . Finding a scale-free distribution in our model is consistent with power laws appearing in the dynamics of the temporal series of tweet activity found in this data set [23] or in structural parameters in similar data sets [18]. Furthermore, our statistical models allow us to find further evidence of the critical behaviour of the model by computing its heat capacity. By introducing a fictitious temperature value by changing the temperature parameter T (previously assumed to be equal to 1), we compute the heat capacity [29] of the system as :

$$C(T) = T \frac{\partial H[P(s)]}{\partial T} = \frac{1}{T^2} \langle E^2(s) \rangle - \langle E(s) \rangle^2 \quad (4)$$

where $H[P(s)]$ is the Shannon entropy of the probability distribution of an Ising model. A peak in the heat capacity of the system is an indicator of critical phenomena. As we observe in Figure 3.B, for all f_k the peak of the heat capacity is around the

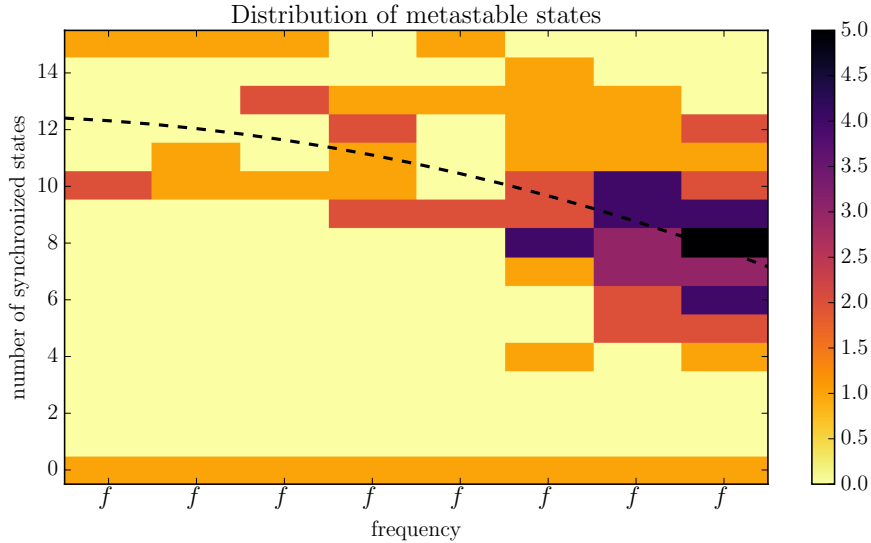


Figure 4. Distribution of metastable states by frequency and synchronized nodes. Distribution of the number of active (i.e. synchronized) states of the inferred Ising models for each frequency band. The horizontal axis represents the frequency band, the vertical axis the number of active states of the metastable states and the color represents the count of metastable states with the same number of active states. The dashed line is the result of a least squares second order polynomial fit over the number of active nodes of metastable states (excluding states with zero active nodes) respect to the frequency index, showing a decrease of the number of synchronized nodes in the metastable states in favour of local clusters of activity.

value $T = 1$ indicating that the models are poised just at critical points. Together with the Zipf distribution, the peaks in heat capacity strongly suggest that social coordination phenomena in the 15M social network are operating at a regime of criticality.

Nevertheless, the fact that all frequency bands are operating in a regime of criticality does not mean that they are displaying the same behaviour. We can extract more information about the behaviour of the system at each frequency by analyzing the presence of locally-stable or metastable states in the system. Metastable states are defined as states whose energy is lower than any of its adjacent states, where adjacency is defined by single spin flips. This means that in a deterministic state (i.e. a Hopfield network with $T = 0$) these points would act as attractors of the system. In our statistical model metastable states are points in which the system tends to be poised, since their probability is higher than any of its adjacent states. Detecting the metastable states of the models at each frequency, we observe how the number of metastable states increases with slower frequencies (Figure S4.B), as well as the model presents a higher number of negative (inhibitory) couplings J_{ij} (see Figure S4.A).

Moreover, if we count the number of nodes that are phase-locked (i.e. the sum of all nodes with $s_i = 1$) across metastable states represented in Figure 4 we observe important distinctions among frequency bands. For faster values of f_k there is only a few metastable states: a state where all nodes are not phase-locked (i.e. the system is completely desynchronized), and a few values where almost all nodes are phase locked. Thus, at fast frequencies synchronization rapidly spreads from zero to all nodes in the network. On the other hand, for slower frequencies the number of metastable states starts growing and the number of phase-locked nodes they contain decreases. This shows that slow frequency synchronizations allows the creation of a variety of clusters of partial synchronization, allowing parts of the network to sustain a differentiated behaviour. This suggests that fast and slow synchronization frequencies in the network may operate in complementary regimes, the former rapidly propagating information to all the network, and the latter allowing a variety of configurations responding to specific situations (as the ones observed in the example of the previous section). The presence of distinct modes of critical behaviour at different frequency bands hints that the system might be operating in a state of self-organized criticality, in which frequency bands adaptively regulate each other in order to maintain a global critical behaviour.

Cross-scale interactions in synchronization dynamics

The modellization of phase-locking statistics of the previous section provides us with a characterization of the interactions within frequency bands of phase-locking activity. As well, differences in the metastable states present at each frequency band suggest us what kind of interactions take place between distinct temporal scales. Unfortunately, as our definition of phase locking statistics is restricted to interactions in a same frequency, we cannot use the computed phase locking statistics to directly model inter-scale phase-locking between different frequencies (e.g. 2:1 phase locking). Nevertheless, we can use the

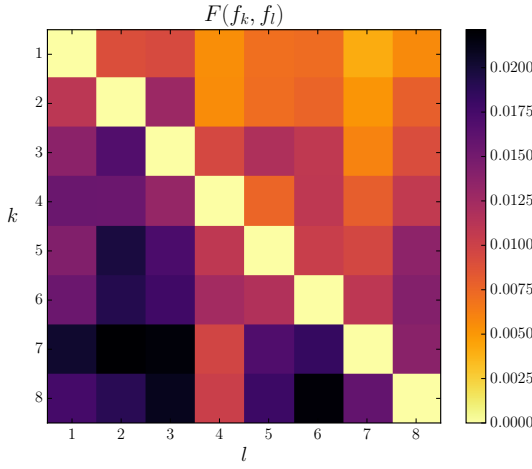
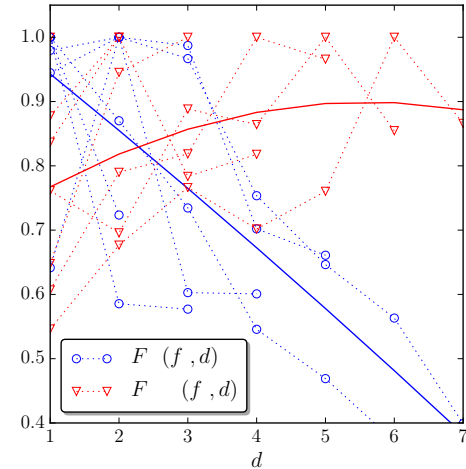
A**B**

Figure 5. Mean transfer entropy. (A) Mean symbolic transfer entropy $F(f_k, f_l)$ across values of τ between energy levels at different frequencies. (B) Tendencies of upward ($F_{up}(f_k, d)$, blue circle markers) and downward ($F_{down}(f_k, d)$, red triangular markers) symbolic transfer entropy values respect to the distance d between frequencies. Solid lines represent a least squares second order polynomial fit of the values of $F_{up}(f_k, d)$ (blue solid line) and $F_{down}(f_k, d)$ (red solid line) respect to d . We observe how upward transfer entropy values display an important decrease with distance, whereas downward transfer entropy presents slightly larger values for larger distances.

thermodynamic descriptions of the system provided by our maximum entropy models to simplify the analysis of inter-scale relations in real data.

Analysis of multiscale causal relations is typically a difficult task, and in our case we have to deal with a system of a high number of dimensions ($15 \cdot 8 = 120$ dimensions). Nevertheless, in our Ising models, the stability of the configurations of the 15 nodes of the network at each frequency band is characterized by an energy value. Thus, an easier way to describe multiscale interactions is to observe how fluctuations in the energy at one level affects the energy of the system at other levels, reducing the dimensions we have to deal with to only our 8 frequencies of synchronization.

We characterize the information flow between frequency bands using symbolic transfer entropy [30] between energy levels at each frequency $E_{f_k}(s(t))$. Symbolic transfer entropy captures the decrease of uncertainty in the state of a variable Y derived from the past state of other variable X :

$$\mathcal{T}_{X \rightarrow Y}(\tau) = \sum_{x_{t+\tau}, x_t, y_t} P(x_{t+\tau}, x_t, y_t) \log \frac{P(x_{t+\tau} | x_t, y_t)}{P(x_{t+\tau} | x_t)} \quad (5)$$

where x_t denotes the state of X and τ indicates the temporal distance used to capture interactions.

In order to compute symbolic transfer entropy over energy values between timescales, we discretize the values of energy $E_{T_l}(s(t))$ into a variable with 3 discrete bins $E_{f_k}^*(s(t))$ using the Jenks-Caspall algorithm [31]. The value of 3 bins was selected to optimize the computation of joint probability density functions (see Supplementary Information) although we tested values from 2 to 6 bins with similar results. Using symbolic transfer entropy we estimate the causal interactions between energetic states at each timescale by computing the values of $\mathcal{T}_{E_{f_k}^* \rightarrow E_{f_l}^*}(\tau)$ (see Supplementary Information for a representation of transfer entropy functions) for values of tau between 1 and 2^9 minutes (i.e. from 1 minute to 8.5 hours) logarithmically distributed with intervals of $2^{0.25}$.

To simplify the interpretation of the data, we compute the mean value of transfer entropy for pairs of frequencies as $F(f_k, f_l) = \langle \mathcal{T}_{E_{f_k}^* \rightarrow E_{f_l}^*}(\tau) \rangle$ (Figure 5.A). Moreover, we separate the values of upward and downward flows of information for each node, characterizing $F_{up}(f_k, d) = F(f_{k-d}, f_k) / \max_d [F(f_{k-d}, f_k)]$ and $F_{down}(f_k, d) = F(f_{k+d}, f_k) / \max_d [F(f_{k+d}, f_k)]$, where d takes values between 1 and 7, and upward and downward entropies are divided by their maximum values in order to compare transfer entropy between nodes with distinct values of entropy. In Figure 5.B, we observe upward and downward flows of information. As we can see, upward flows decrease importantly with distance between scales. On the contrary, downward flows increase slightly with distance between scales.

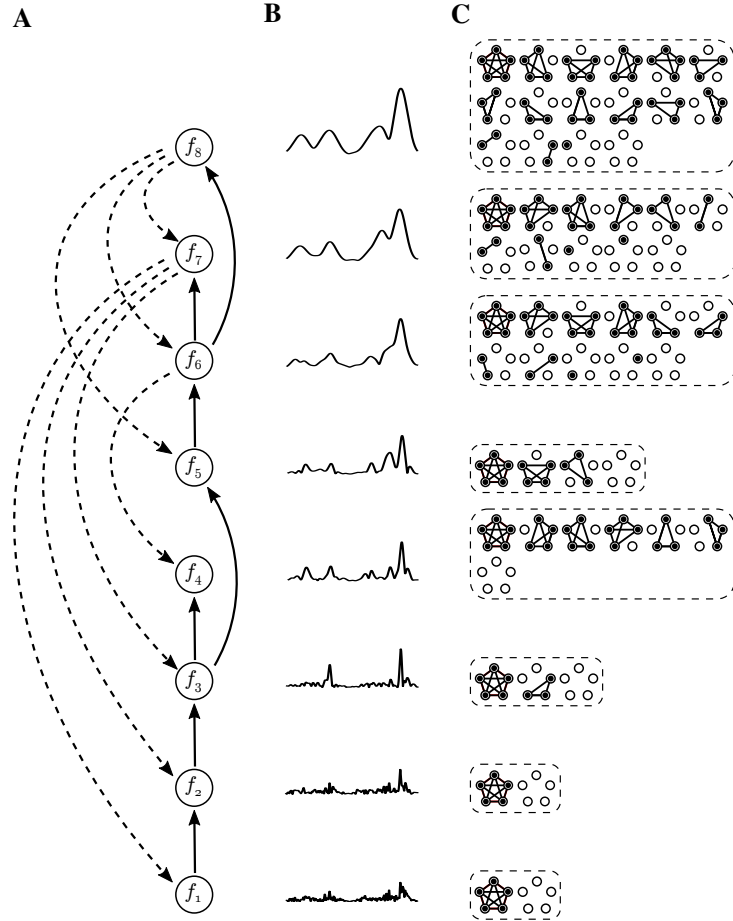


Figure 6. Cross-scale interactions in social coordination. Schematic displaying the results presented in previous figures. (A) Interactions in terms of mean transfer entropy between energy levels at different frequencies described by $F_{up}(f_k, d)$ and $F_{down}(f_k, d)$. For simplicity only the largest upward (solid arrows) and downward (dashed arrows) transfer entropy values are represented. (B) Fragment of activity of all nodes in the network (in number of tweets per second) filtered by the different wavelets used in the filtering of frequency bands. (C) Metastable states of the models at each frequency. For simplicity, only metastable configurations of the five cities with largest total volume of activity are represented.

These results show an interesting picture of cross-scale interactions. While in upward interactions energy at each frequency band only influences neighbouring slower bands, in downward interactions slow frequency bands modulate distant faster bands. We also observe this in the schematic in Figure 6.A, where for simplicity only largest values of $F_{up}(f_k, d)$ and $F_{down}(f_k, d)$ are displayed for each frequency band. These results suggest an asymmetry in cross-scale interactions in which upward influences cascade from faster to slower frequency bands, while slower frequencies in the top of the hierarchy exert a strong influence over fast frequencies at the bottom. This circularity might take a role in sustaining the self-organization of multitudinous social systems by creating a nested structure of frequency bands creating a (temporal) hierarchy in an otherwise distributed system.

Discussion

We have shown how the application of maximum entropy inference methods over phase-locking statistics at different frequencies in data from social media offers the opportunity to understand collective phenomena at a deeper level. First, inferring Ising models describing phase-locking statistics between geographical nodes at different frequency bands we have shown how each band operates in a regime of criticality displaying distinct modes of behaviour. While fast frequency bands present a few metastable states switching between (almost) full synchronization and full desynchronization, slower frequency bands present an increasing number of metastable states showing a myriad of configurations with partial synchrony. This suggests that fast frequency bands rapidly spread information through the network in moments of full synchronization, while slower bands are

able to sustain configurations of differentiated activity between nodes of the network, balancing integration and differentiation of geographical nodes. Second, the set of inferred Ising models allows us to tackle the more difficult task of analyzing cross-scale interactions between frequency bands. Using symbolic transfer entropy to observe causal interactions between energy levels at each frequency band, we observe an asymmetry between upward and downward flows of information. While upward flows correspond mostly to frequency bands influencing adjacent slower bands, in downward flows slow frequencies modulate distant fast frequencies. This asymmetry may constitute a mechanism for maintaining the self-organization of the system, in which flows of upward information are filtered from smaller to larger timescales of coordination, while these large scales of coordination are able to exert a downward modulation of all inferior levels.

The presented results provide interesting insights about the self-organization of digitally connected multitudes and how are these networks activated, structured and maintained in the absence of recognized leaders or fixed common goals. Our contribution suggests that phase-locking mechanisms at different frequencies may act as a metastable mechanism for integrating the activity of the network at fast frequencies while maintaining a diversity of distinct configurations at slower frequencies. Moreover, the asymmetry between upward and downward flows of information suggests how social systems operating through distributed transient synchronization may create a hierarchical structure of temporal timescales, in which hierarchy is not reflected in a centralized control but in the asymmetry of information flows between the coordinative structures at different frequencies of activity. This offers a suggestive explanation of how an unified collective agency might emerge in a distributed manner from mechanisms of transient large-scale synchronization.

Methods

Data preprocessing

We use a data set of 1,444,051 tweets from 181,146 users, collected between 13 May 2011 and 31 May 2011. This data set [16] was extracted from the Twitter streaming API, which provides information on the time and content of the tweet, as well as information on the sender, including location. Messages were captured when they contained one of the following hashtags or keywords (which were selected as some of the most relevant during the emergence of the 15M movement): #15M, 15-M, #democraciarealya, #tomalacalle, #Nolesvotes, #spanishrevolution, #acampadasol, #acampadabcn, #indignados, #notenemosmiedo, #nonosvamos, #yeswecamp. We filter messages in the data set using the location field in the description of the user that sent the message. Since the 15M was (at least during the first days) mainly an urban phenomena, we analyse geographical interactions between the 15 cities with more activity in Twitter during 17 days of the protests. We find the 15 names of cities most repeated in the data set, and counted messages corresponding to a specific city when the city name appeared in the location field. Since the location is a field of the description of the user, it does not necessarily correspond to the real location of the user at the moment the message was sent. We ran a test on geolocalized Twitter data from Spain, observing that for a set of 20.000 random tweets in a 80.25% the profile location corresponds with the actual geolocation of the user, giving the information of the user's location field a moderately high reliability.

Data availability

The data employed in this study was kindly provided by the authors of reference 16.

Phase-locking statistics

Time series of activity at each city are generated by counting the number of messages from users located at the city in intervals of 60 seconds for a period comprising a period of 17 days, starting at 2AM May 14th 2011. Each time series is filtered using Morlet wavelets at different frequencies. For each city i and frequency f we extract the phase content $\theta_x(f, t)$ for each moment of time t , with a frequency span between $[1.67 \cdot 10^{-3} \text{Hz}, 9.26 \cdot 10^{-5} \text{Hz}]$ (from 10 minutes to 3 hours) mapped into a logarithmic sequence with intervals of $10^{0.01}$.

Phase-locking values are defined for each pair of cities i and j as defined in Equation 1. We introduce a corrector factor $A_{ij}(t)$ to remove spurious synchronization when the network is inactive. $A_{ij}(t)$ is zero when the mean activity of nodes i or j for a moving window of 30 minutes is below a threshold of 0.25 times its mean activation, which generally happened during some periods at night.

From phase-locking values we extract phase-locking links, which are activated when the phase-locking value is higher than 99% of a set of 200 surrogate time series we generate for purposes of statistical validation, as indicated in Equation 2. Surrogate time series are generated using amplitude adjusted Fourier transform using the TISEAN software (Available at http://www.mpiipks-dresden.mpg.de/~tisean/Tisean_3.0.1/). Amplitude adjusted Fourier transform surrogates [22] are time series that preserve the power spectrum of a distribution and a distribution of values, but remove the temporal correlations present in the original signal.

Results shown in Figure 2 (described in detail in reference 23), we measured transfer entropy as in Equation 5 signals $\theta_x(f, t)$ and $\theta_y(f, t)$ for the two most salient values of f , where phase values were discretized to binary values depending if

$\sin(\theta_x(f, t) - \frac{1}{N} \sum_{x'=1}^N \theta_{x'}(f, t))$ was positive or negative.

Detection of synchronization frequency bands

We localize frequency bands synchronization by detecting peaks of salient phase-locking links in the logarithmic frequency space. We compute the mean synchronization for each frequency as the temporal mean of phase locking links at that frequency $S(f) = \langle \sum_{i,j} \Phi_{ij}(f, t) \rangle$. In order to robustly detect peaks, we remove the loglinear trend present in $S(f)$ and apply a two-dimensional wavelet transform [27]. Using Ricker wavelets from withs from 1 to 10 over the vector of logarithmic frequencies, eight peaks where found by identifying the ridge lines in the wavelet transform matrix. Each timescale is described obtaining the frequency of each peak and computing its period $T_p = \frac{1}{f_p}$, where $p = 1, \dots, 8$ are the indices of the 8 peaks of salient synchronization (See Supplementary Information for detailed results).

Learning pairwise maximum entropy models from data

In order to infer a maximum entropy model from the data, the activation of each node of the system as the presence of at least one phase-locking link. For each value of t and f , $s_i = 1$ if $\sum_j \Phi_{ij}(f, t) > 0$, or $s_i = -1$ otherwise. Thus, we consider a node as active when it is phase-locked to a synchronized cluster, and inactive when the node is desynchronized from the rest of the network. For each timescale of oscillation, we inferred a Ising model as described in Equation 3, using an adapted verios of the coordinate descent algorithm described in reference 32. The coordinate descent algorithm works by iteratively adjusting a single weight h_i or J_{ij} that will maximize an approximation of the change in the empirical logarithmic loss between the observed data and the model, computed through the means and correlations present in the empirical data and the model. The code implementing the coordinate descent algorithm is available at <https://github.com/MiguelAguilera/ising>.

References

1. W. H. McNeill, *Keeping Together in Time: Dance and Drill in Human History*. New York, USA: ACLS Humanities E-Book, Aug. 2008.
2. K. Hill, “Anabaptism and the World of Printing in Sixteenth-Century Germany,” *Past & Present*, vol. 226, pp. 79–114, Feb. 2015.
3. D. Chang, Y. Ge, S. Song, N. Coleman, J. Christensen, and J. Heer, “Visualizing the Republic of Letters,” *Stanford: Stanford University. Retrieved April*, vol. 21, p. 2014, 2009.
4. M. Castells, “Communication, Power and Counter-power in the Network Society,” *International Journal of Communication*, vol. 1, p. 29, Feb. 2007.
5. P. Levy, *Collective Intelligence: Mankind’s Emerging World in Cyberspace*. Perseus Books, 1999.
6. H. Rheingold, *Smart Mobs: The Next Social Revolution*. Basic Books, Mar. 2007.
7. W. L. Bennett, A. Segerberg, and S. Walker, “Organization in the crowd: peer production in large-scale networked protests,” *Information, Communication & Society*, vol. 17, pp. 232–260, Feb. 2014.
8. W. L. Bennett and A. Segerberg, “The logic of connective action: Digital media and the personalization of contentious politics,” *Information, Communication & Society*, vol. 15, no. 5, pp. 739–768, 2012.
9. J. S. Juris, “Reflections on #Occupy Everywhere: Social media, public space, and emerging logics of aggregation,” *American Ethnologist*, vol. 39, pp. 259–279, May 2012.
10. P. Gerbaudo, “Online aggregation in the ‘mass web’,” 2013.
11. F. Varela, J.-P. Lachaux, E. Rodriguez, and J. Martinerie, “The brainweb: Phase synchronization and large-scale integration,” *Nature Reviews Neuroscience*, vol. 2, pp. 229–239, Apr. 2001.
12. M. Le Van Quyen, “The brainweb of cross-scale interactions,” *New Ideas in Psychology*, vol. 29, pp. 57–63, Aug. 2011.
13. A. Monterde, A. Calleja-López, M. Aguilera, X. E. Barandiaran, and J. Postill, “Multitudinous identities: a qualitative and network analysis of the 15m collective identity,” *Information, Communication & Society*, vol. 18, pp. 930–950, Aug. 2015.
14. D. Lazer, A. Pentland, L. Adamic, S. Aral, A.-L. Barabási, D. Brewer, N. Christakis, N. Contractor, J. Fowler, M. Gutmann, T. Jebara, G. King, M. Macy, D. Roy, and M. V. Alstyne, “Computational Social,” *Science*, vol. 323, pp. 721–723, Feb. 2009.
15. V. Sampedro and J. Lobera, “The Spanish 15-M Movement: a consensual dissent?,” *Journal of Spanish Cultural Studies*, vol. 15, pp. 61–80, Apr. 2014.

16. I. Peña-López, M. Congosto, and P. Aragón, “Spanish Indignados and the evolution of the 15m movement on Twitter: towards networked para-institutions,” *Journal of Spanish Cultural Studies*, vol. 15, pp. 189–216, Apr. 2014.
17. S. Tormey and R. A. Feenstra, “Reinventing the political party in Spain: the case of 15m and the Spanish mobilisations,” *Policy Studies*, vol. 36, pp. 590–606, Nov. 2015.
18. J. Borge-Holthoefer, A. Rivero, I. García, E. Cauhé, A. Ferrer, D. Ferrer, D. Francos, D. Iñiguez, M. P. Pérez, G. Ruiz, F. Sanz, F. Serrano, C. Viñas, A. Tarancón, and Y. Moreno, “Structural and Dynamical Patterns on Online Social Networks: The Spanish May 15th Movement as a Case Study,” *PLoS ONE*, vol. 6, p. e23883, Aug. 2011.
19. S. González-Bailón, J. Borge-Holthoefer, A. Rivero, and Y. Moreno, “The Dynamics of Protest Recruitment through an Online Network,” *Scientific Reports*, vol. 1, Dec. 2011.
20. J. Borge-Holthoefer, N. Perra, B. Gonçalves, S. González-Bailón, A. Arenas, Y. Moreno, and A. Vespignani, “The dynamic of information-driven coordination phenomena: a transfer entropy analysis,” *arXiv:1507.06106 [nlin, physics:physics]*, July 2015. arXiv: 1507.06106.
21. J.-P. Lachaux, E. Rodriguez, M. Le Van Quyen, A. Lutz, J. Martinerie, and F. J. Varela, “Studying single-trials of phase synchronous activity in the brain,” *International Journal of Bifurcation and Chaos*, vol. 10, no. 10, pp. 2429–2439, 2000.
22. T. Schreiber and A. Schmitz, “Improved Surrogate Data for Nonlinearity Tests,” *Physical Review Letters*, vol. 77, pp. 635–638, July 1996.
23. M. Aguilera, “The Collective Mind: large-scale self-organization in social systems,” in *Interaction dynamics and autonomy in cognitive systems*, Tesis de la Universidad de Zaragoza, pp. 211–248, Universidad de Zaragoza, 2015.
24. E. Schneidman, M. J. Berry, R. Segev, and W. Bialek, “Weak pairwise correlations imply strongly correlated network states in a neural population,” *Nature*, vol. 440, pp. 1007–1012, Apr. 2006.
25. T. Mora, A. M. Walczak, W. Bialek, and C. G. Callan, “Maximum entropy models for antibody diversity,” *Proceedings of the National Academy of Sciences*, vol. 107, pp. 5405–5410, Mar. 2010.
26. W. Bialek, A. Cavagna, I. Giardina, T. Mora, E. Silvestri, M. Viale, and A. M. Walczak, “Statistical mechanics for natural flocks of birds,” *Proceedings of the National Academy of Sciences*, vol. 109, pp. 4786–4791, Mar. 2012.
27. P. Du, W. A. Kibbe, and S. M. Lin, “Improved peak detection in mass spectrum by incorporating continuous wavelet transform-based pattern matching,” *Bioinformatics*, vol. 22, pp. 2059–2065, Sept. 2006.
28. T. Mora and W. Bialek, “Are biological systems poised at criticality?,” *Journal of Statistical Physics*, vol. 144, no. 2, pp. 268–302, 2011.
29. T. Mora, S. Deny, and O. Marre, “Dynamical Criticality in the Collective Activity of a Population of Retinal Neurons,” *Physical Review Letters*, vol. 114, p. 078105, Feb. 2015.
30. T. Schreiber, “Measuring Information Transfer,” *Physical Review Letters*, vol. 85, pp. 461–464, July 2000.
31. G. F. Jenks and F. C. Caspall, “Error on Choroplethic Maps: Definition, Measurement, Reduction,” *Annals of the Association of American Geographers*, vol. 61, pp. 217–244, June 1971.
32. M. Dudík, S. J. Phillips, and R. E. Schapire, “Performance Guarantees for Regularized Maximum Entropy Density Estimation,” in *Learning Theory* (J. Shawe-Taylor and Y. Singer, eds.), no. 3120 in Lecture Notes in Computer Science, pp. 472–486, Springer Berlin Heidelberg, July 2004.

Acknowledgements

This research has been partially supported by the project PSI2014-62092-EXP of the National Programme for Fostering Excellence in Scientific and Technical Research ('Explora Ciencia' call) from the Spanish Ministry of Economy and Competitiveness.

Supplementary Information

Detection of salient synchronization frequency bands

We localize frequency bands synchronization by detecting peaks of salient phase-locking links in the logarithmic frequency space. We compute the mean number of synchronization links for each frequency as the temporal mean of phase locking links at that frequency $S(f) = \langle \sum_{i,j} \Phi_{ij}(f, t) \rangle$ (Figure S1.A). As $S(f)$ increases with slower frequencies following approximately a log-linear trend, we approximate the trend, we compute a least squares first order polynomial fit respect to the logarithm of f and remove it from $S(f)$. In order to robustly detect peaks, we apply a two-dimensional wavelet transform of the detrended $S(f)$ over the vector of logarithmic frequencies. Using 10 Ricker wavelets of widths from 1 to 10 steps in the selected logarithmic range of frequency (i.e. a range of $[1.67 \cdot 10^{-3} \text{Hz}, 9.26 \cdot 10^{-5} \text{Hz}]$ logarithmically distributed with intervals of $10^{0.01}$) we compute the wavelet transform matrix and detect its ridge lines to find eight peaks of salient synchronization (code available at https://github.com/scipy/scipy/blob/v0.14.0/scipy/signal/_peak_finding.py#L410). As the position of the detected peaks vary slightly depending on the parameters employed, we adjust the position of each peaks by climbing to the nearest local maxima if one is found within a distance of two steps. In Figure S1.B we observe the result of the process and the 8 detected peaks. From these peaks we extract 8 frequencies f_k , with $k = 1, \dots, 8$, indicating the position of the peaks in $S(f)$ (Table S1).

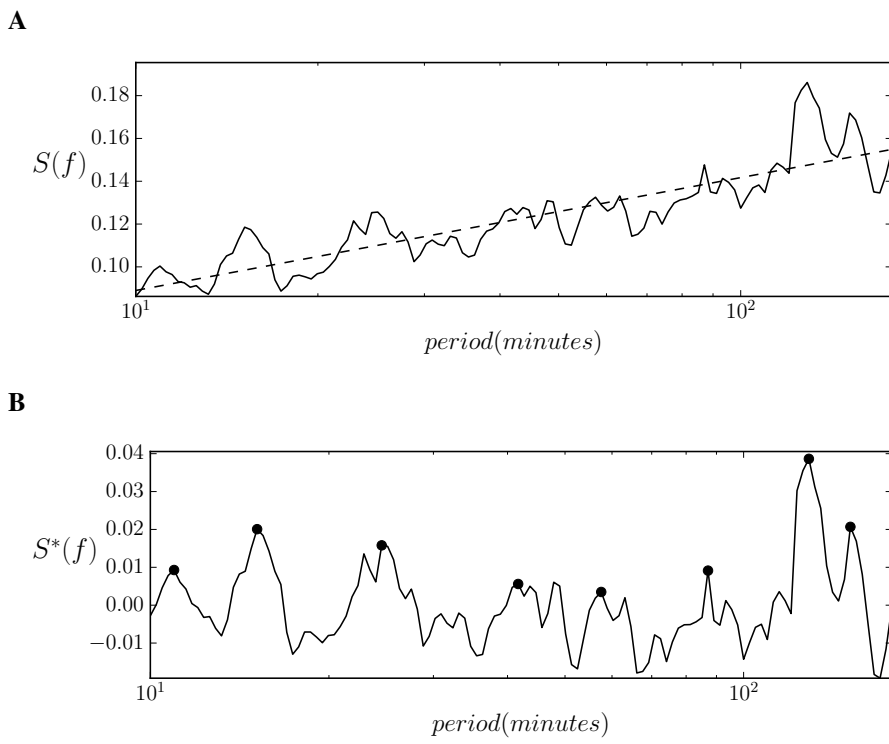


Figure S1. Peaks of salient synchronization. (A) Sum of total phase locking links $S(f)$ for each value of frequency (solid line). We detect a log-linear trend that we remove for detecting synchronization peaks. (B) Detrended $S(f)$ for each value of frequency (solid line). Synchronization peaks found using a two-dimensional wavelet transform (black dots).

Number of samples required to compute probability distributions

When we compute multi-informations and symbolic transfer entropies, we face a compromise between the size of our probability distribution functions and the number of samples we employ for describing them. In order to correctly compute these probability distributions, we need to ensure that the number of samples found in our data is sufficiently large for describing the frequency of occurrence of all possible states. Although the number of samples in our data is large, as data changes at different frequencies, slower frequencies may present a smaller number of transitions between states than fast frequencies, therefore offering a reduced effective sample of visited states.

In order to quantify the number of states visited at each frequency, we count the number of transitions between states s used to infer the Ising models at each frequency (Table S2). Knowing that number, we can estimate a threshold of how many states

Label	Frequency
f_1	1.52e-3Hz
f_2	1.10e-3Hz
f_3	6.78e-4Hz
f_4	4.00e-4Hz
f_5	2.90e-4Hz
f_6	1.91e-4Hz
f_7	1.29e-4Hz
f_8	1.10e-4Hz

Table S1. Frequencies of salient synchronization. Table representing the frequency values corresponding to the peaks represented in Figure S1.B.

can have a probability distribution to be accurately estimated from our samples at different frequencies. We arbitrarily establish a requirement of the number of transitions being larger than 2^4 times the number of possible states of the objective probability distribution function. Although the exact value of the threshold is arbitrary, during the analysis we tried different thresholds to ensure the robustness of the results.

Frequency	f_1	f_2	f_3	f_4	f_5	f_6	f_7	f_8
Number of transitions between states	2276	1903	1387	922	865	692	731	641

Table S2. Number of state transitions for each frequency. Number of transitions between states s from the data used for computing the Ising model at each selected frequency. S2.

Multi-information measures for assessing the accuracy of maximum entropy models

Once we infer the maximum entropy models that correspond to the means and correlations found in phase-locking data, it is important to characterize what is the accuracy of the model, that is, to what extent the statistical model generated is mapping the data we used in the inference. The accuracy of the model can be further evaluated by asking how much of the correlative structure found in the data is captured. We can measure the overall strength of correlations in the network using multi-information, which is defined as the total reduction in entropy relative to an independent model $I = H[P_1] - H[P_r]$, where $H[P_r]$ is the entropy of the distribution of the real system whose data we are analyzing and $H[P_1]$ is the entropy of an independent model. In our case, an independent model would be the equivalent of adjusting an Ising model in which the couplings are zero, and thus its energy function is defined as $E(s) = -\sum_i h_i s_i$. Multi-information can as well be used to compute the reduction of entropy of the distributions P_2 of the pairwise Ising model we inferred from data as $I_2 = H[P_1] - H[P_2]$. The ratio between these two quantities gives the fraction of the correlations captured by the pairwise Ising model:

$$\frac{I_2}{I} = \frac{H[P_1] - H[P_2]}{H[P_1] - H[P_r]} \quad (1)$$

Unfortunately, the data available is not enough for reliably computing P_r . The probability distribution P_r has a number of possible states of 2^{15} , while in our data the number of different states transited by the system is one or two orders of magnitude inferior, depending on the frequency. However, we can compute accurately subsets of the complete probability distribution $P_r(s'_i)$, with $\{s'_i\} \subset \{s_i\}$. For each frequency, we count the number of transitions between states found in the time series in our data, and contrast that number with the dimension of the subset of the probability function using a number n of nodes, i.e. 2^n . We use an arbitrary threshold requiring the number of states being at least 2^4 times larger than the number of values of the probability distribution function. Different thresholds yield slightly different results, although they don't change significantly the final results. We find that for frequencies from f_4 to f_8 we can compute reliably subsets with up to 5 nodes. For frequencies f_2 and f_3 the number increases to up to 6 and for f_7 it is 7 nodes.

In Figure S2 we can observe the distribution of the values of $\frac{I_2}{I}$ for 100 random choices of subsets for each number of nodes. We can observe that most of the subsets the values of $\frac{I_2}{I}$ indicate that between 60% and 80% of the correlations are captured (Table S3)

The limited availability of data, specially for slower frequencies, prevents us to compute the accuracy of the model for subsets with larger number of nodes. Future analysis applied to larger data sets should test if the accuracy of the model holds for capturing the correlations between larger subsets of nodes.

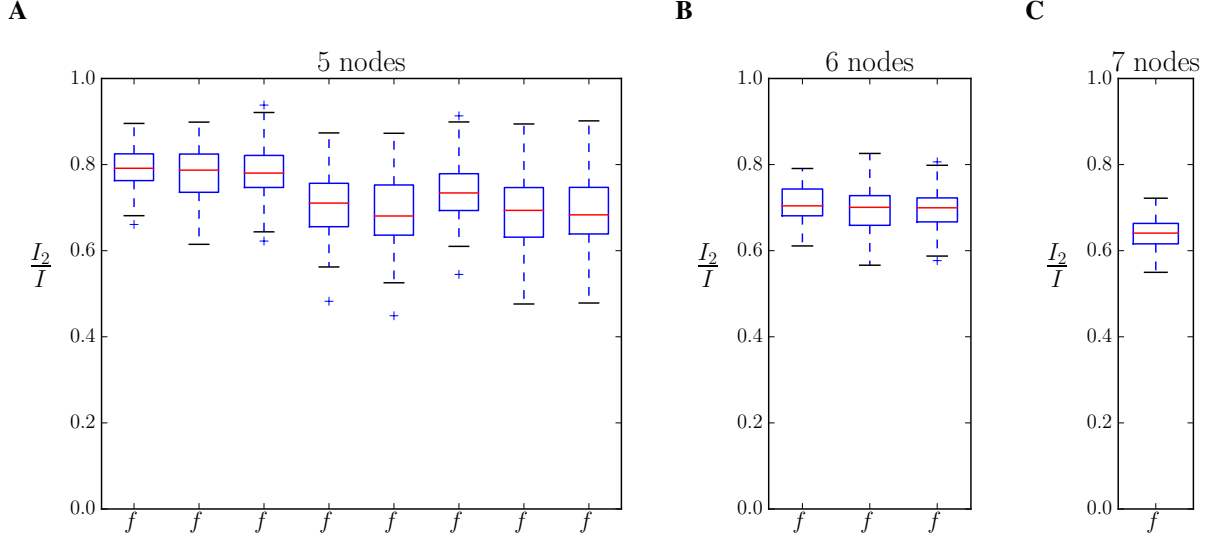


Figure S2. Accuracy of the model. Values of $\frac{I_2}{I}$ for subsets of combinations of nodes at each frequency. Each boxplot represents the distribution of $\frac{I_2}{I}$ for 100 subsets of n nodes at a specific frequency band selected randomly comparing the multi-information of the model and real data.

Frequency	$n = 5$	$n = 6$	$n = 7$
f_1	$\mu = 0.790, \sigma = 0.0493$	$\mu = 0.707, \sigma = 0.0434$	$\mu = 0.696, \sigma = 0.0341$
f_2	$\mu = 0.778, \sigma = 0.0596$	$\mu = 0.696, \sigma = 0.0520$	
f_3	$\mu = 0.782, \sigma = 0.0602$	$\mu = 0.698, \sigma = 0.0497$	
f_4	$\mu = 0.707, \sigma = 0.0748$		
f_5	$\mu = 0.692, \sigma = 0.0832$		
f_6	$\mu = 0.739, \sigma = 0.0693$		
f_7	$\mu = 0.685, \sigma = 0.0863$		
f_8	$\mu = 0.687, \sigma = 0.0928$		

Table S3. Distributions of multi-information ratios. Mean and standard deviation for each distribution in Figure S2.

Parameters of the Ising models

Here we display the parameters h and J inferred for the Ising models at each frequency. As we observe in Figure S3, as we move from faster to slower frequencies, the amplitude of h and J increases. As well, the percentage of negative couplings increases. We compute the ratio of negative couplings as:

$$r_{\text{neg}} = \frac{0.5 \sum_{i < j} (J_{ij} - |J_{ij}|)}{\sum_{i < j} |J_{ij}|} \quad (2)$$

On figure S4.A we can observe how the ratio of negative coupling increases with slower frequencies. It is known from spin glass theory that metastable states emerge when some of the couplings between variables are negative. In Figure S4 we can observe how there is a correlation between the ratio of negative couplings and the number of metastable states.

Transfer Entropy

Using the energy of the Ising models E_{f_k} at different frequencies, we compute symbolic transfer entropy by discretizing energy functions into clusterized variables $E_{f_k}^*$. We apply natural Break classification through the Jenks-Caspall algorithm (code available at <https://github.com/domlysz/Jenks-Caspall.py>), which for each cluster minimizes the average deviation from the cluster's mean to determine the best arrangement of values into different clusters. Since computing transfer entropies requires to compute joint probability functions with three variables, to meet the same criteria we used to compute multi-information, we use a number of 3 clusters to ensure that for all the frequencies we have a number of samples of transited states which is at least 2^4 times larger than the values in the probability distribution. After discretizing the energy functions we

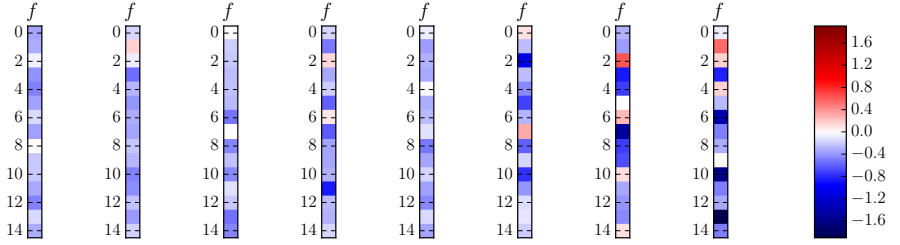
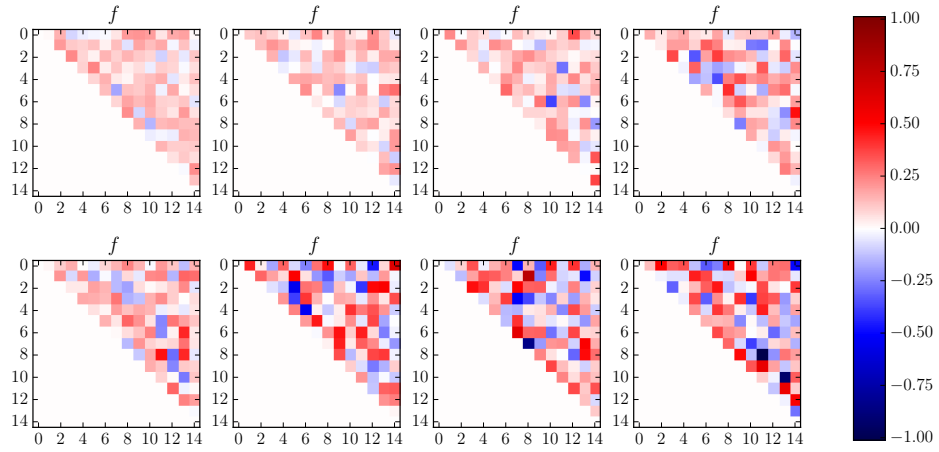
A**B**

Figure S3. Parameters of the Ising models. For each frequency, we depict the parameters h (A) and J (B) of the inferred Ising models.

compute the values of symbolic transfer entropies $\mathcal{T}_{kl}(\tau) = \mathcal{T}_{E_{f_k}^* \rightarrow E_{f_l}^*}(\tau)$ for values of τ in a range between $[1, 2^8]$ (i.e. from 1 minute to more than 4 hours) logarithmically distributed with intervals of $2^{0.25}$. Functions $\mathcal{T}_{kl}(\tau) = \mathcal{T}_{E_{f_k}^* \rightarrow E_{f_l}^*}(\tau)$ for different values of k and l are represented in Figure S5

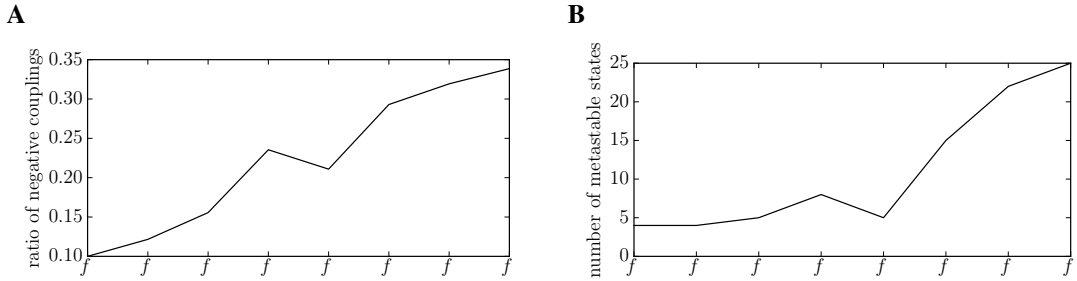


Figure S4. Negative couplings and number of metastable states. (A) Ratio of negative couplings for the inferred values of J_{ij} for each frequency. (B) Count of the number of metastable states for each frequency.

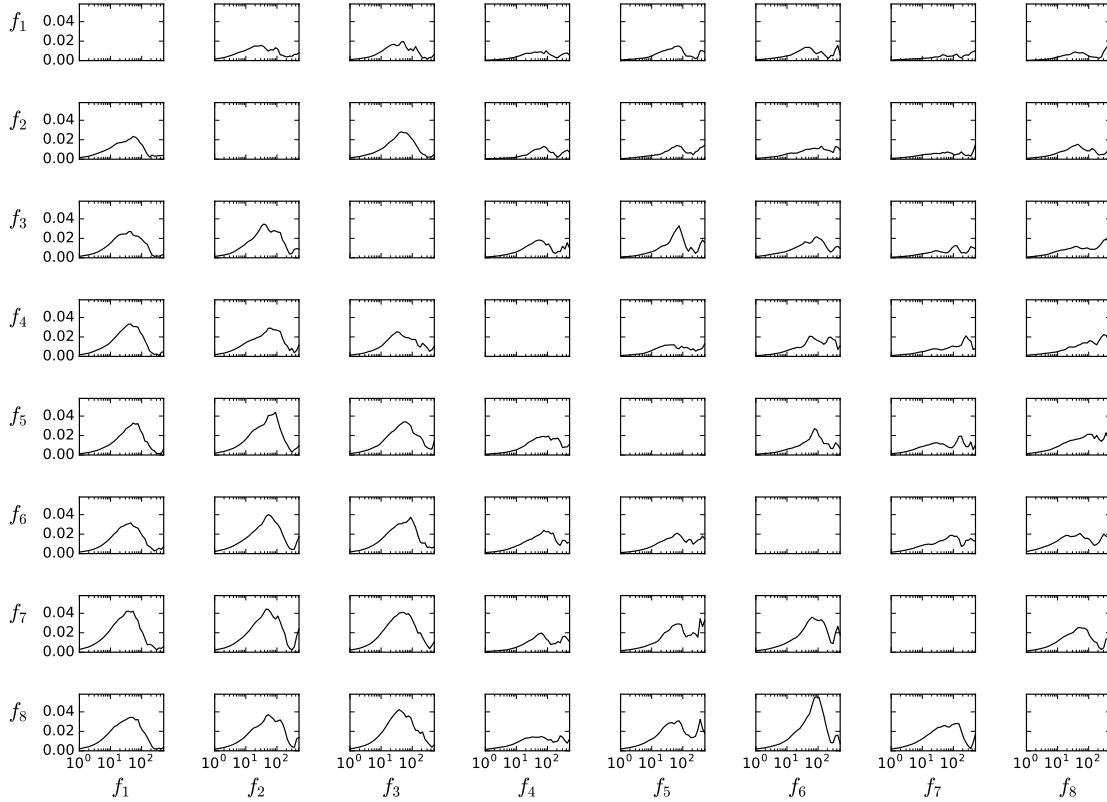


Figure S5. Transfer entropy. We represent functions $\mathcal{T}_{kl}(\tau) = \mathcal{T}_{E_{f_k}^* \rightarrow E_{f_l}^*}(\tau)$ for values of τ in a range between $[1, 2^9]$ (i.e. from 1 minute to 8.5 hours) logarithmically distributed with intervals of $2^{0.25}$. Rows specify the value of f_k while columns specify the value of f_l . For each graph, the vertical axis represents the value of symbolic transfer entropy and the horizontal axis the value of τ in minutes.